



Study of surface layers and ejected powder formed by oxidation of titanium substrates with a pulsed Nd:YAG laser beam

I. Shupyk^{a,*}, L. Lavissee^{a,*}, J.-M. Jouvard^a, M.C. Marco de Lucas^a, S. Bourgeois^a,
F. Herbst^b, J.-Y. Piquemal^b, F. Bozon-Verduraz^b, M. Pilloz^a

^a Institut Carnot de Bourgogne, UMR 5209 CNRS-Université de Bourgogne, 9 Av. A. Savary, BP 47 870, F-21078 Dijon Cedex, France

^b ITODYS, UMR CNRS 7086, Université Paris Diderot - Paris 7, Bâtiment Lavoisier, 15 rue Jean de Baïf, 75205 Paris Cedex 13, France

ARTICLE INFO

Article history:

Received 6 June 2008

Received in revised form 28 August 2008

Accepted 28 August 2008

Available online 12 September 2008

Keywords:

Laser treatments

Plasma

Titanium dioxide

Nanoparticles

ABSTRACT

Laser treatment of a titanium surface at certain conditions initiates the formation of titanium oxide layers as well as micro (nano) scale powder ejected from the surface of the substrate. The resultant morphology of the surface as well as the size and the structure of the particles are all strongly dependent on the treatment parameters (laser fluence, pulse frequency, overlap parameter, etc.). In this study, titanium substrates were treated with an industrial pulsed Nd:YAG laser in air, with varying parameters. Surface layers and ejected materials were compared using scanning and transmission electron microscopy, X-ray diffraction and Raman spectroscopy. The rutile phase of TiO₂ dominates in the surface layers, while the ejected powder is mainly formed of anatase nanoparticles.

© 2008 Elsevier B.V. All rights reserved.

1. Introduction

The titanium surface modification with Nd:YAG pulsed laser beam followed by microstructural study was reported in previous publications [1,2]. It was shown that surface state of a material is strongly influenced by the laser treatment parameter and experimental conditions: e.g. oxygen insertion during laser irradiation of titanium surface in air is mainly influenced by repetition rate, while nitrogen insertion is controlled by laser fluence [3]. By varying of laser fluence it is also possible to obtain the colored layers (yellow, blue, purple) on titanium surface, characterized by different morphologies, structures and chemical compositions [2,4]. Moreover, the formation of a thick oxidized layer at the titanium surface by a laser treatment can significantly improve the tribological properties of titanium [5,6].

In addition to modifications of the surface state of the titanium substrate, depending on laser treatment, powder can be ejected from the surface. Deposition of powder ejected from a target by

laser beam is used in widely applied pulsed laser deposition (PLD) method for TiO₂ films preparation [7,8].

In this work, we are interested in the study of laser treatments of titanium substrates, with experimental conditions (laser current intensity and pulse frequency) leading to strong oxidation of titanium surface. Results concerning both the oxidized surface layers and powder ejected during laser treatments are reported in this paper and compared to each other.

2. Experimental details

2.1. Titanium substrates

Commercially pure grade 4 titanium (Cezus) samples dimensions of 15 mm × 10 mm × 3 mm were used as substrates. Before laser treatment the titanium surface was mechanically polished in order to remove the contaminants and surface oxide layer and to obtain very smooth metal surface (Ra < 0.5 μm).

2.2. Laser treatments

The industrial Roфин Sinar SLM40D Q-switch Nd:YAG marking laser (λ = 1.064 μm; pulse duration 190–360 ns) was applied for laser treatment of titanium substrates in air. Prior to the samples preparation a preliminary study was realized in wide range of laser

* Corresponding authors at: Institut Carnot de Bourgogne, UMR 5209 CNRS – Université de Bourgogne, 12 rue de la Fonderie, 71200 Le Creusot, France. Tel.: +33 3 85 73 10 56; fax: +33 3 85 73 11 20.

E-mail addresses: ishupyk@yahoo.fr (I. Shupyk), luc.lavissee@u-bourgogne.fr (L. Lavissee).

Table 1

Laser treatment parameters used for preparing two series of samples: (i) series TI (surface layers) and TIP (powder), where T, titanium; I, indicated current intensity; P, ejected powder, and (ii) series Tf (surface layers) and TFP (powder), where T, titanium; f, pulse frequency with indicated experimental values; P, ejected powder.

Sample	I (A)	f (kHz)	τ (ns)	P_1 (W)	F_{1p}^a (J cm ⁻²)	I_p^b (MW cm ⁻²)	σ^c	F^d (kJ cm ⁻²)
T35 (P)	35	15.5	335	31.1	2.5	7	3174	7.9
T40 (P)	40	15.5	300	44.5	3.6	12	3174	11.4
T45 (P)	45	15.5	270	56.6	4.5	17	3174	14.3
T50 (P)	50	15.5	240	67.5	5.4	22	3174	17.1
Tf5.5 (P)	40	5.5	190	36.5	8.2	43	1126	9.2
Tf9.5 (P)	40	9.5	280	42.0	5.5	19	1946	10.7
Tf13.5 (P)	40	13.5	290	43.7	4.0	13	2765	11.1
Tf19.5 (P)	40	19.5	330	46.0	3.0	9	3994	11.9
Tf23.5 (P)	40	23.5	360	47.2	2.5	7	4813	12.0

^a $F_{1p} = P_1/(Af)$, where F_{1p} , laser fluence per pulse (J cm⁻²); P_1 , the average laser power (W); A , laser spot area (cm²); f , pulse frequency (s⁻¹) [2].

^b $I_p = F_{1p}/\tau$, where I_p , laser light intensity (W cm⁻²); F_{1p} , laser fluence per pulse (J cm⁻²); τ , pulse duration (s).

^c $\sigma = \phi^2 f / (vd)$, where σ , overlap parameter (dimensionless); ϕ , laser spot diameter (m); f , pulse frequency (s⁻¹); v , laser scanning speed (m s⁻¹); d , distance between two consecutive lines (m) [19];

^d $F = F_{1p}\sigma$, where F , accumulated fluence (kJ cm⁻²).

treatment parameters in order to define the optimal conditions leading to essential oxidation of titanium surface. Following this study, the two sets of samples (Table 1) were prepared (i) by varying the current intensity, I , in the range of 35–50 A with a pulse frequency fixed at $f = 15.5$ kHz (series TI (surface layers) and TIP (powder)); where T, titanium; I , indicated current intensity; P, ejected powder) and (ii) by varying the frequency from 5.5 up to 23.5 kHz at $I = 40$ A (series Tf (surface layers) and TFP (powder)); where T, titanium; f , pulse frequency with indicated experimental values; P, ejected powder).

The two glass plates (25 mm × 25 mm) were used for ejected powder deposition as shown at Fig. 1.

2.3. Characterization techniques

Scanning electron microscopy (SEM) studies were done with a JEOL JSM 6400F apparatus typically working at 20 keV.

High-resolution transmission electron microscopy (HRTEM) was performed using a JEOL JEM 2010 transmission electron

microscope operating at 200 kV acceleration voltage and equipped with a PGT Imix-PC system.

X-ray diffraction patterns (Co K α radiation; $\lambda = 1.78901$ Å) were recorded on a PANalytical X'Pert Pro diffractometer equipped with a X'celerator detector. The patterns were analyzed using X'Pert Highscore software developed by PANalytical and with Profit software developed by Philips. The crystallite size for anatase and rutile phases was determined using the Debye-Scherrer formula. The weight fraction of the rutile phase was estimated according to the Spurr's formula [9].

Raman spectra were obtained with a Jobin-Yvon T64000 micro-Raman spectrometer. The spectra were obtained in back-scattering configuration with a spatial resolution of about 1 μ m. The excitation was provided by an Ar-Kr ion laser. The wavelength was 514.5 nm and the excitation power was about 400 μ W that is low enough to avoid heating the samples.

3. Results and discussion

3.1. SEM and TEM results

The morphology of the oxidized surface layers was observed by optical microscopy and SEM (not shown here). According to these techniques, the oxidized surface layer exhibits a marked roughness and displays the traces of the laser scanning lines.

SEM images of ejected powder, deposited on the glass plates, reveal formation of a continuous layer composed of nanoscale particles less than 30–50 nm (Fig. 2d). In addition, some bigger particles (micron scale) were also observed, but only for powders on the glass plate, located at short distance (~ 5 mm) from the target surface (Fig. 2b and c). These results can be explained by different sources of powder formation: the nanoparticles are probably formed in the plasma plume [10,11] while the bigger ones, droplet shaped, are directly ejected by the laser impacts from the melting bath formed at the titanium surface under applied laser light intensities (Table 1) [12].

The nanoparticles in the continuous layer of ejected powder were further studied by transmission electron microscopy (TEM). The TEM image corresponding to the sample T40P is shown in Fig. 3a. It demonstrates that TiO₂ nanoparticles are uniformly and homogeneously dispersed, with an average particle size of about 11 nm. Moreover, HRTEM images show that the particles are very well crystallized and belong to the anatase phase (see electron diffraction pattern, Fig. 3b, inset).

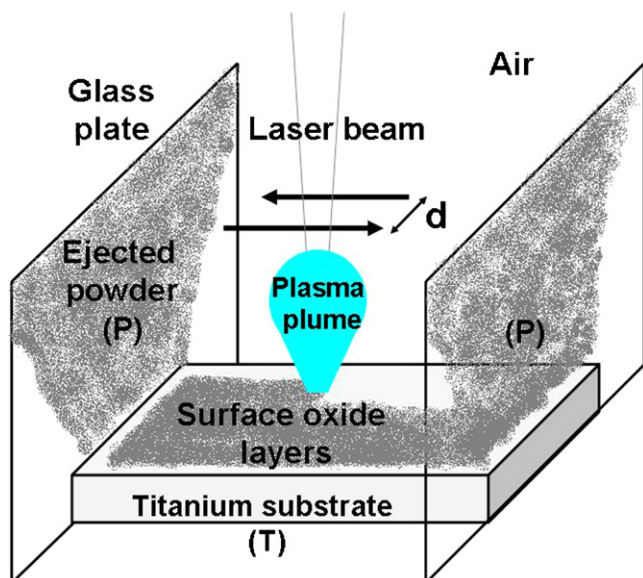


Fig. 1. Schematic representation of the laser treatment of titanium surface and powder deposition. T and P stand for titanium substrate (15 mm × 10 mm × 3 mm) and powder deposited on the glass plates (25 mm × 25 mm), respectively. The parallel straight lines were made on titanium surface by the laser beam ($\phi = 320$ μ m) with a scanning speed, $v = 10$ mm s⁻¹, and distance between two consecutive lines, $d = 50$ μ m. The laser treated area was 12 mm × 8 mm.

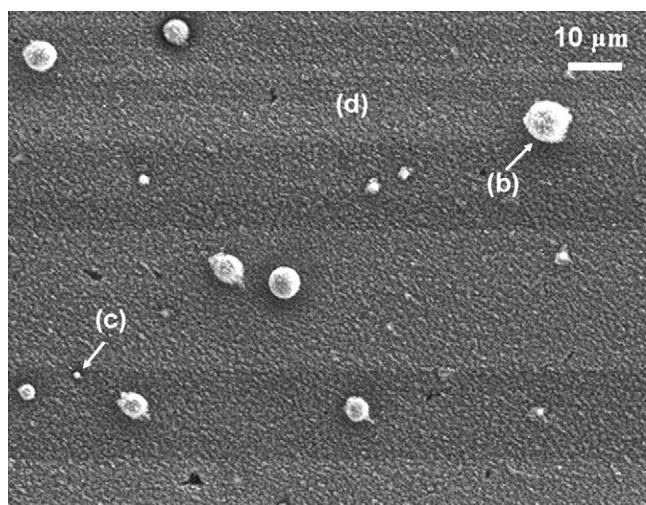


Fig. 2. SEM image of the ejected powder, deposited on the glass plate (T40P). The image was taken from the zone close to the target's surface (~5 mm). Labels (b–d) indicate characteristic zones corresponding in Fig. 5 to the Raman spectra b, c and d, respectively.

3.2. X-ray diffraction results

The XRD patterns (Fig. 4) reveal a main difference between the oxide surface layers and ejected powder. Thus titanium surface

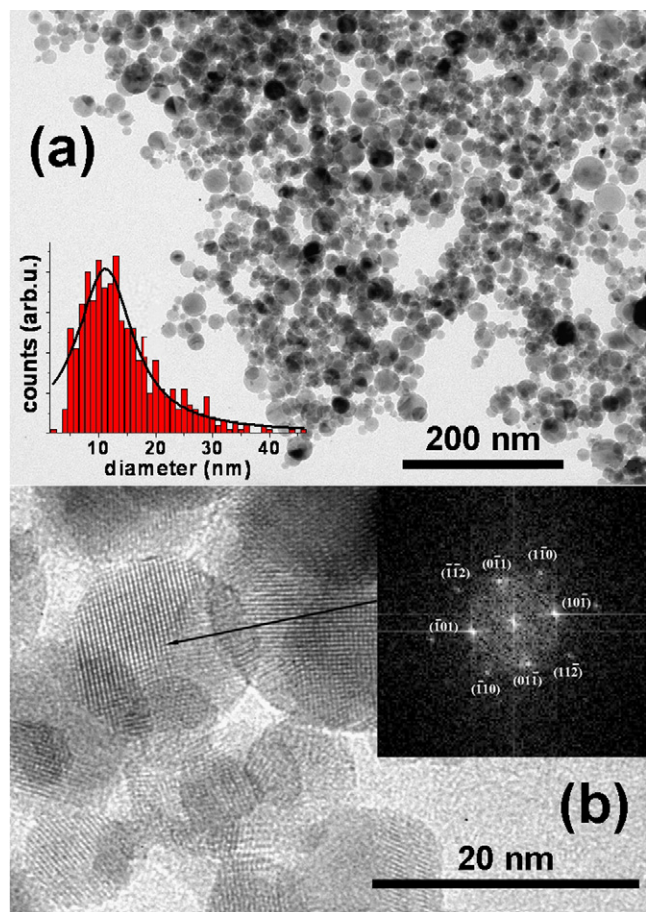


Fig. 3. TEM image of continuous layer of ejected powder (T40P) with a particles size distribution graph (a); HRTEM image with diffraction pattern, indexed according to the anatase axis of zone (1 1 1) (b).

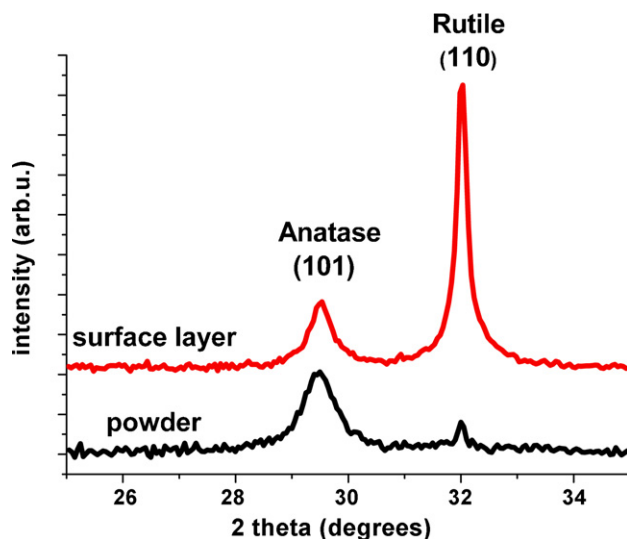


Fig. 4. XRD patterns of surface oxide layer (T40) and ejected powder deposited on the glass plate (T40P). Short 2 theta domain displays the two most intense peaks of anatase and rutile phases of TiO_2 .

upon laser treatment shows mainly the rutile phase of TiO_2 and minor amount of anatase, while the powder deposited on the glass plates exhibits anatase as a main crystallographic phase with very small amounts of rutile, as it was also shown by HRTEM.

The rutile and anatase mean crystallite sizes are represented in Table 2 only for layers and powder, respectively, because in most cases the small amount of rutile in powder or anatase in the surface layers does not allow a correct determination of the FWHM values from diffraction peaks used in Debye-Scherrer formula.

It was found, that increasing the laser fluence by varying the current intensity at a fixed frequency (series TI) enhances the weight percentage of the rutile phase (Table 2) in the surface layers from about 50% to 90%. The same tendency is observed for the size of rutile crystallites (36–107 nm) that increases with higher laser fluence.

Nevertheless, the amount of rutile found in ejected powder (series TIP) was low (not higher than 10%), while anatase was dominant phase with the size of crystallites 12–15 nm.

The metastable anatase form of TiO_2 can be transformed into stable rutile by thermal treatment in the 600–1000 °C range [13,14]. This process is accompanied by increasing of the size of

Table 2

Rutile (D_{110}) and anatase (D_{101}) mean crystallite size in the surface layers and ejected powder, respectively, and rutile percentage (X) calculated from the XRD patterns.

Sample	Rutile ^a D_{110} (nm)	Anatase D_{101} (nm)	^b X (%)	
	Layer	Powder	Layer	Powder
T35 (P)	36 ± 4	12 ± 2	~50	–
T40 (P)	52 ± 3	14 ± 2	~75	~10
T45 (P)	67 ± 4	14 ± 2	~80	~10
T50 (P)	107 ± 2	15 ± 1	~90	~10
Tf5.5 (P)	41 ± 3	11 ± 2	~70	~40
Tf9.5 (P)	46 ± 2	13 ± 2	~75	~25
Tf13.5 (P)	43 ± 2	13 ± 2	~75	~10
Tf19.5 (P)	147 ± 4	13 ± 2	~80	~10
Tf23.5 (P)	153 ± 2	10 ± 2	~95	–

^a $D_{hkl} = 0.9\lambda / (\beta_{hkl} \cos \theta)$, where D_{hkl} is the crystallite size, λ the X-ray wavelength, β_{hkl} the corrected FWHM from high-purity silicon and θ is the Bragg angle for the (hkl) diffraction peak.

^b $X = [A_R / (A_R + 0.884A_A)] \times 100$, where X , weight percentage of rutile (%); A_A and A_R are the areas under the (1 0 1) diffraction peak of anatase phase and the (1 1 0) peak of rutile phase, respectively [9].

anatase crystallites that at some critical value (about 15 nm) start to transform into rutile [15,16]. In the case of this laser treatment, the more energy was deposited, the higher rutile content and rutile crystallites size were found in the surface oxide layers.

The variation of the pulse frequency at a fixed current intensity was also analyzed (series Tf). According to Table 1, upon increasing pulse frequency, the laser fluence per pulse (F_{1p}) decreases, but the accumulated fluence (F) increases due to the high values of the overlap parameter. Such conditions induce a high rutile content (about 70–95%) in the surface oxide layers, which increases with the pulse frequency, as it is also the case for the rutile crystallites size (41–153 nm).

On the contrary, the amount of rutile is low in the ejected powder (series TfP) and it decreases by increasing the pulse frequency. In fact, no rutile was found for the highest frequency (Tf23.5P). At the same time, the anatase crystallite size (10–13 nm) compares well with the first series of samples obtained by varying the current intensity.

3.3. Raman spectroscopy

Micro-Raman spectra recorded in different points of the oxidized surface layer show the growth of TiO₂ in the rutile phase together

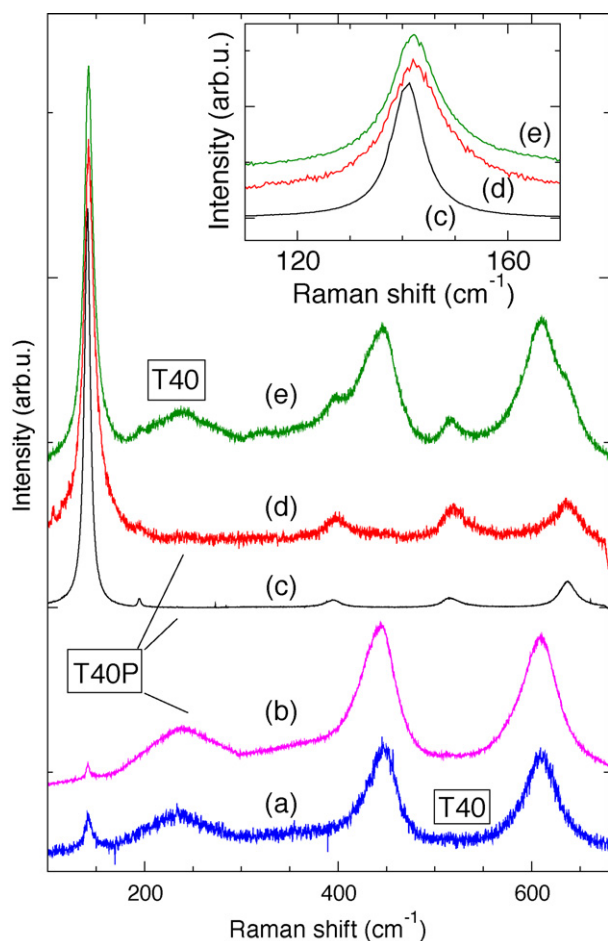


Fig. 5. Raman spectra recorded in different areas of the oxidized surface layer (a and e) and the ejected powder (b–d) for the samples T40 and T40P, respectively. Spectra (b) and (c) correspond to different micron scale particles observed by optical microscopy in the ejected powder deposited on a glass plate, while spectrum (d) corresponds to the continuous layer of nanoparticles observed in the same sample. The inset shows a magnification of spectra (c–e) in the range of the most intense band of the anatase phase. The spectra were vertically shifted for the sake of clarity.

with a lower amount of the anatase phase (Fig. 5), as it was found by XRD experiments. The anatase phase displays five Raman bands located at 142 (high), 197 (very small), 400, 514 and 639 cm⁻¹, while the rutile phase displays four Raman bands located at 143 (very small), 447, 612 and 826 cm⁻¹ [17]. The spectrum of the rutile phase was mainly found when analyzing the lowest zones of the rough layer surface (Fig. 5a). On the other hand, the peaks associated with the anatase phase were detected together with those of the rutile phase when analyzing the highest zones (Fig. 5e).

The study of the ejected powder deposited on a glass plate showed different Raman spectra for the continuous layer (Fig. 2d) and for the isolated micron scale particles observed by SEM and optical microscopy. For the latter ones (Fig. 2b), the intensity of the Raman signal was high and it was mainly associated with the rutile phase (Fig. 5b), though the anatase phase was found (Fig. 5c) in some of these micron scale crystallites (Fig. 2c).

For the continuous layer composed of nanoscale particles, the intensity of the Raman signal was low and the spectrum displays only the bands associated to the anatase phase (Fig. 5d), which is in agreement with HRTEM results. Moreover, the fraction of rutile phase in the ejected powder estimated from the XRD pattern was very low. It is worth noting the shift (~ 1 cm⁻¹) and the broadening (~ 6 cm⁻¹) of the most intense band of the anatase phase with respect to the spectrum obtained for the anatase phase in micron scale particles (Fig. 5c). Many works have been devoted to study the shift and the broadening of this band as a function of the anatase particles size in the nanometer scale [18]. Here, the values of the shift and the broadening of this band correspond to a particle size about 12 nm, in agreement with HRTEM observations and XRD pattern analyses. Moreover, a similar shift and broadening can also be observed in the spectrum (e) of Fig. 5 which was obtained in highest zones of the layer formed at the surface of the Ti target. Note that the size estimated by XRD was about 20 nm. All these results suggest that anatase nanoparticles are formed in the plasma above the target before being deposited on the glass plates and also on the top of the oxidized target.

4. Conclusion

The realized treatments of Ti substrates with a pulsed Nd:YAG laser beam in air induced a strong oxidation of titanium surface together with ejection of the micro- and nanosized TiO₂ powders.

The crystallographic structure and the crystallite size of the oxidation products (layers and powder) are strongly influenced by the laser parameters, i.e. current intensity and pulse frequency.

The rutile phase is predominant in the surface layers, while the ejected powder is mainly formed of anatase nanoparticles. In the surface oxide layers, the weight percentage of rutile and the rutile mean crystallite size increase with the laser current intensity and the pulse frequency, i.e. increasing accumulated fluence.

Conversely, for ejected powders, no significant variation of the anatase particle size is observed. Moreover, decreasing of laser fluence per pulse with high pulse frequency leads to decreasing of the rutile weight percentage even at high accumulated fluence.

Acknowledgements

I. Shupyk acknowledges the financial support of this work provided by EGIDE and Conseil Régional de Bourgogne, France. Claudie Josse is gratefully acknowledged for the SEM experiments.

References

- [1] L. Lavisie, D. Grevey, C. Langlade, B. Vannes, Appl. Surf. Sci. 186 (2002) 150.
- [2] L. Lavisie, J.-M. Jouvard, L. Imhoff, O. Heintz, J. Korntheuer, C. Langlade, S. Bourgeois, M.C. Marco de Lucas, Appl. Surf. Sci. 253 (2007) 8226.

- [3] L. Lavis, J.-M. Jouvard, J.P. Gallien, P. Berger, D. Grevey, Ph. Naudy, *Appl. Surf. Sci.* 254 (2007) 916.
- [4] A. Pérez del Pino, P. Serra, J.L. Morenza, *Thin Solid Films* 415 (2002) 201.
- [5] M.C. Marco de Lucas, L. Lavis, G. Pillon, *Tribol. Int.* 41 (2008) 985.
- [6] C. Langlade, A.B. Vannes, J.M. Krafft, J.R. Martin, *Surf. Coat. Tech.* 100–101 (1998) 383.
- [7] L.C. Chen, in: D.B. Chrisey, G.K. Hubler (Eds.), *Pulsed Laser Deposition of Thin Films*, Wiley, 1994, p. 195.
- [8] S.I. Kitazawa, Y. Choi, S. Yamamoto, T. Yamaki, *Thin Solid Films* 515 (2006) 1901.
- [9] R.A. Spurr, H. Myers, *Anal. Chem.* 29 (1957) 760.
- [10] T. Ohshima, S. Nakashima, T. Ueda, H. Kawasaki, Y. Suda, K. Ebihara, *Thin Solid Films* 506–507 (2006) 106.
- [11] T.E. Itina, M. Sentis, W. Marine, *Appl. Surf. Sci.* 252 (2006) 4433.
- [12] D. Bäuerle, *Laser Processing and Chemistry*, second ed., Springer, Berlin, 1996, p. 6.
- [13] Y. Hu, H.-L. Tsai, C.L. Huang, *Mater. Sci. Eng. A* 344 (2003) 209.
- [14] C.-S. Kim, I.-M. Kwon, B.K. Moon, J.H. Jeong, B.-C. Choi, J.H. Kim, H. Choi, S.S. Yi, D.-H. Yoo, K.-S. Hong, J.-H. Park, H.S. Lee, *Mater. Sci. Eng. C* 27 (2007) 1343.
- [15] A. Orendorz, A. Brodyanski, J. Löscher, L.H. Bai, Z.H. Chen, Y.K. Le, C. Ziegler, H. Gnaser, *Surf. Sci.* 601 (2007) 4390.
- [16] H. Zhang, J.F. Banfield, *J. Mater. Chem.* 8 (1998) 2073.
- [17] A. Pottier, S. Cassaignon, C. Chaneac, F. Villain, *J. Mater. Chem.* 13 (2003) 877.
- [18] D. Bersani, P.P. Lottici, X.-Z. Ding, *Appl. Phys. Lett.* 72 (1998) 73.
- [19] D. Höche, G. Rapin, J. Kaspar, M. Shinn, P. Schaaf, *Appl. Surf. Sci.* 253 (2007) 8041.